NEOPLASIA
www.neoplasia.com

Volume 10 Number 5 May 2008 pp. 511–520 511

Bevacizumab Inhibits Breast Cancer–Induced Osteolysis, Surrounding Soft Tissue Metastasis, and Angiogenesis in Rats as Visualized by VCT and MRI[1]

Tobias Bäuerle*,†, Heidegard Hilbig‡, Sönke Bartling†, Fabian Kiessling†, Astrid Kersten§, Annette Schmitt-Gräff§, Hans-Ulrich Kauczor*, Stefan Delorme* and Martin R. Berger¶

*Department of Radiology, German Cancer Research Center, Im Neuenheimer Feld 280, 69120 Heidelberg, Germany; †Department of Medical Physics in Radiology, German Cancer Research Center, Im Neuenheimer Feld 280, 69120 Heidelberg, Germany; ‡Institute of Anatomy, University of Leipzig, Liebigstraße 13, 04103 Leipzig, Germany; §Institute of Pathology, University of Freiburg, Breisacher Straße 115a, 79002 Freiburg, Germany; ¶Chemotherapy and Toxicology Unit, German Cancer Research Center, Im Neuenheimer Feld 280, 69120 Heidelberg, Germany

Abstract

The aim of this study was to evaluate the effect of an antiangiogenic treatment with the vascular endothelial growth factor antibody bevacizumab in an experimental model of breast cancer bone metastasis and to monitor osteolysis, soft tissue tumor, and angiogenesis in bone metastasis noninvasively by volumetric computed tomography (VCT) and magnetic resonance imaging (MRI). After inoculation of MDA-MB-231 human breast cancer cells into nude rats, bone metastasis was monitored with contrast-enhanced VCT and MRI from day 30 to day 70 after tumor cell inoculation, respectively. Thereby, animals of the treatment group (10 mg/kg bevacizumab IV weekly, $n = 15$) were compared with sham-treated animals ($n = 17$). Treatment with bevacizumab resulted in a significant difference versus control in osteolytic as well as soft tissue lesion sizes (days 50 to 70 and 40 to 70 after tumor cell inoculation, respectively; $P < .05$). This observation was paralleled with significantly reduced vascularization in the treatment group as shown by reduced increase in relative signal intensity in dynamic contrast-enhanced MRI from days 40 to 70 ($P < .05$). Contrast-enhanced VCT and histology confirmed decreased angiogenesis as well as new bone formation after application of bevacizumab. In conclusion, bevacizumab significantly inhibited osteolysis, surrounding soft tissue tumor growth, and angiogenesis in an experimental model of breast cancer bone metastasis as visualized by VCT and MRI.

Neoplasia (2008) 10, 511–520

Introduction

Bone metastasis is a frequent complication of breast and prostate malignancies, which are among the most common carcinomas in women and men. Compared with patients with other generalized neoplasias, patients with breast cancer bone metastasis experience a relatively long median survival time of 20 months after diagnosis of skeletal involvement [1]. Because skeletal complications including pathologic fractures, hypercalcemia, and bone pain in these patients can be severe, new treatment options that expand the therapeutic arsenal beyond currently available options are desirable.

Abbreviations: DCE, dynamic contrast enhanced; GFP, green fluorescent protein; MRI, magnetic resonance imaging; p.i., postinjection; UICC, International Union Against Cancer; VCT, volumetric computed tomography; VEGF, vascular endothelial growth factor

Address all correspondence to: Martin R. Berger, Chemotherapy and Toxicology Unit, German Cancer Research Center, Im Neuenheimer Feld 280, 69120 Heidelberg, Germany. E-mail: m.berger@dkfz.de

[1]This study was supported by a grant from "Deutsche Krebshilfe e.V." (Bonn, Germany).
Received 25 January 2008; Revised 18 February 2008; Accepted 20 February 2008

DOI 10.1593/neo.08220

A promising target is cancer-related angiogenesis, which is also required in bone metastasis as the tumor grows beyond a certain size [2]. In line with this, angiogenesis was observed in bone marrow of patients with breast cancer and was associated with progression or recurrence of disease [3]. However, angiogenesis and antiangiogenic treatment have not been studied systematically in breast cancer bone metastasis. Furthermore, no animal model of breast cancer bone metastasis has been described that allows one to follow angiogenesis noninvasively *in vivo*.

Angiogenesis is an essential feature of cancer growth and an increasing number of factors are known to be involved. Among these, vascular endothelial growth factor (VEGF) and its isotypes play a crucial role [4]. Interestingly, serum levels of VEGF in patients with breast cancer were significantly increased in patients with bone metastases but not in those with localized disease [5]. In experimental models of breast cancer bone metastasis, VEGF was found to be associated with expression of bone-resorption stimulators and, consequently, osteoclast-mediated osteolysis [6].

However, because skeletal lesions caused by tumor growth are relatively late events in the pathogenesis of bone metastasis the monitoring of soft tissue–associated processes preceding bone destruction is desirable. These processes include, for example, angiogenesis in bone metastasis, which has not been visualized before. So far, for imaging of tumor angiogenesis in breast and liver lesions, dynamic contrast-enhanced (DCE) magnetic resonance imaging (MRI) is being used in patients with cancer and has become the standard imaging technique [7]. In tumors, DCE MRI can noninvasively assess vascularization and evaluate the drug efficacy of antiangiogenic agents [7]. For small-animal research, contrast-enhanced volumetric computed tomography (VCT) has been developed as a fast and high-resolution imaging of new vessel formation in tumors [8,9].

The aim of this study was to combine these approaches by evaluating the effect of an antiangiogenic treatment with an antibody against VEGF and by imaging noninvasively the treatment effects on osteolysis, surrounding soft tissue tumor, and angiogenesis in a preclinical model of breast cancer bone metastasis in nude rats.

Materials and Methods

Cell Lines and Culture Conditions

The human estrogen-independent breast cancer cell line MDA-MB-231 was obtained from the American Type Culture Collection. MDA-MB-231 cells stably transfected with green fluorescent protein (GFP) (pEGFP-N1; Clontech, Mountain View, CA) were kindly provided by Dr. Danny R. Welch (Pennsylvania State University College of Medicine, Hershey, PA). Tumor cells were cultured routinely in RPMI 1640 (Invitrogen, Karlsruhe, Germany) supplemented with 10% fetal calf serum (Sigma, Taufkirchen, Germany). All cultures were kept under standard conditions (37°C, humidified atmosphere, 5% CO_2) and passaged two to three times a week to keep them in logarithmic growth.

Animals and Husbandry

Nude rats (RNU strain) were obtained from Harlan Winkelmann (Borchen, Germany) at an age of 6 to 8 weeks. They were housed two per cage at specific pathogen-free conditions in a minibarrier system of the central animal facility. Autoclaved feed and water were given *ad libitum* to the animals that were maintained under controlled conditions (21 ± 2°C room temperature, 60% humidity, and 12-hour light-dark rhythm). Experiments were approved by the responsible governmental animal ethics committee (Regierungspräsidium Karlsruhe, Germany).

In Vivo *Metastasis Model*

Subconfluent MDA-MB-231 tumor cells were harvested using 2 mM EDTA in PBS^- (phosphate-buffered saline without Ca^{2+} and Mg^{2+}) and 0.25% trypsin (Sigma, Taufkirchen, Germany). Cells were counted in a Neubauer's chamber and suspended in RPMI 1640 (5×10^5 cells in 1 ml). For tumor cell implantation, rats were anesthetized with a mixture of nitrous oxide (1 l/min), oxygen (0.5 l/min), and isoflurane (1 to 1.5 vol %). For tumor cell inoculation (method of inoculation described in Ref. [10]) the arterial branches of the right hind leg were dissected. A needle was inserted into the superficial epigastric artery, which is branching off the femoral artery, and 10^5 MDA-MB-231 cells suspended in 0.2 ml RPMI 1640 were injected. Vessel clips were used to direct the tumor cells to the descending genicular and popliteal arteries, which supply the knee joint and the muscles of the leg. Resulting bone metastases were observed exclusively in the femur, tibia, and fibula of the respective hind leg [10].

In Vivo *Imaging*

For *in vivo* imaging with VCT and MRI, rats were anesthetized with nitrous oxide, oxygen, and isoflurane as stated above.

Volumetric computed tomography. VCT imaging was performed on a flat panel–equipped volumetric computed tomograph (Volume CT, Siemens, Germany) on days 30, 40, 50, 60, and 70 after tumor cell inoculation, with the following parameters: tube voltage 80 kV, tube current 50 mA, scan time 51 seconds, rotation speed 10 seconds (five rotations per scan), 120 frames per second, 512 × 512 matrix, and 0.2-cm slice thickness. For each animal, contrast agent (1 g iodine per kilogram; Imeron 400, Bracco, Milan, Italy) was injected intravenously on day 70 after tumor cell inoculation during the second rotation of the flat panel system (to acquire an unenhanced data set at first for comparison with the contrast-enhanced data set). Reconstructions of the images were done with VCT Reconstruction (kernel H80a, Afra, Germany). Imaging data of the bone (VCT without contrast agent) and the tumor vessels (VCT after contrast agent injection) in those animals were reconstructed with Osirix (Osirix Dicom Viewer, Version 2.7.5; The Osirix Foundation, Geneva, Switzerland). For comparison of vessel branching patterns between the groups, the number of altered vessels (newly formed vessels or vessels showing an increase in diameter) was counted in control and treated animals.

Magnetic resonance imaging. Magnetic resonance images were acquired on a 1.5-T MR scanner (Symphony, Siemens, Germany) on days 30, 40, 50, 60, and 70 after tumor cell inoculation (anesthesia as given above) using a home-built coil for radiofrequency excitation and detection, designed as a cylindrical volume resonator with an inner diameter of 83 mm and a usable length of 120 mm [11]. The animals were imaged with T2-weighted turbo spin-echo sequences (orientation axial, TR 3240 milliseconds, TE 81 milliseconds, matrix 152 × 256, FOV 90 × 53.4 mm^2, slice thickness 1.5 mm, number of slices 15, three averages, scan time 3 minutes 40 seconds; orientation sagittal, TR 3240 milliseconds, TE 72 milliseconds, matrix 108 × 256, FOV 150 × 63.3 mm^2, slice thickness 2 mm,

number of slices 10, three averages, scan time 2 minutes 40 seconds) and a saturation recovery turbo flash sequence through the largest diameter of the tumor (orientation axial, TR 373 milliseconds, TE 1.86 milliseconds, matrix 192 × 144, FOV 130 × 97.5 mm^2, slice thickness 5 mm, measurements 512, average 1, scan time 6 minutes 55 seconds) while 0.1 mmol/kg Gd-DTPA (Magnevist, Schering, Germany) was infused over a period of 10 seconds. After the infusion of the Gd-DTPA, signal intensity–time curves were recorded. Analysis of the dynamic data was based on the pharmacokinetic two-compartment model of Brix et al. [12]. In this model, compartment 1 represents the intravascular volume and compartment 2 the extravascular, extracellular space. The relative change in signal intensity after contrast media infusion in these two compartments is reflected by the amplitude *A*. Algorithms for calculation of the amplitude *A* were implemented in the computer-based software Dyna Lab (Mevis Research, Bremen, Germany) [11,12]. With the aid of this software tool, color maps of *A* were calculated on axial slices showing the greatest extent of metastasis. After placing a region of interest around the soft tissue metastasis on these color maps the *A* values (arbitrary units) were determined.

The osteolytic lesion and the soft tissue tumor size were determined on unenhanced VCT and MR images by the cross product of the length of the lesion in the direction of the affected bone and its longest perpendicular diameter (in millimeters squared). According to the criteria for assessment of disease response in bone metastases from the International Union Against Cancer (UICC), these lesions were categorized as follows: complete response (disappearance of all known lesions), partial response (at least 50% decrease in size), no change (between 25% increase and 50% decrease in size), and progressive disease (more than 50% increase in size) [13]. Measurements of the bone metastases including osteolytic lesion size, soft tissue tumor size, and amplitude *A* were done by two observers (T.B. and S.B.) in consensus. Absolute values were recorded for the osteolytic lesion and soft tissue tumor sizes (in millimeters squared) as well as for the amplitude *A* in arbitrary units on days 30 to 70 after tumor cell inoculation. Each of these absolute values was transferred into percent of the value at day 30 (100%).

Anti-VEGF Antibody

The monoclonal anti-VEGF antibody bevacizumab (Avastin, Roche, Basel, Switzerland) was administered (10 mg/kg IV) weekly to the nude rats of the treatment group on days 35, 42, 49, 56, and 63 after tumor cell inoculation. Tumor-bearing control animals received saline injections instead of bevacizumab.

Statistical Analyses

For each animal, the lesion sizes for osteolysis and soft tissue tumor as well as the values for the amplitude *A* and the number of altered vessels obtained from VCT and MR imaging were used to draw a curve versus time after tumor cell inoculation. From these numbers, relative values (%) were calculated referring to the initial values on day 30 for each animal. For statistical comparisons, these relative values were compared between the control and treatment groups with the two-sided Wilcoxon test. P values < .05 were considered significant. For comparison between the numbers of animals of each UICC category (progressive disease, no change, partial response, complete response) the χ^2 test was applied, considering P values < .05 significant.

Bone Storage and Histology

Animals were sacrificed on day 70 after tumor cell inoculation. The lower limbs from each animal were excised at sacrifice and the surrounding tissue was stripped off. After fixation in 70% ethanol, the specimens were decalcified in 10% buffered EDTA, pH 7.4, for 3 days. The specimens were cut parallel to the long axis, dehydrated in a series of ethanol (70%, 80%, 90%, 100%) and xylene, and embedded in paraffin wax by routine protocols. Sections of tissue blocks (3 μm in thickness) were deparaffinized, rehydrated, and stained with Mayer's hematoxylin and eosin for histologic evaluation. Serial sections were mounted onto coated SuperFrost Plus glass microscope slides (Langenbeck, Germany) for further immunohistochemical analyses.

After being rinsed for 5 minutes with tap water for immunohistochemical staining, the sections were rinsed several times with 0.1 M PBS (pH 7.4) and incubated with 10% normal donkey serum (Vector, Burlingame, CA) diluted in PBS for 2 hours. Thereafter, the sections were incubated overnight with the antibody against rat CD31 (goat polyclonal PECAM-1, Santa Cruz Biotechnology, Santa Cruz, CA), which was diluted 1:100 in PBS containing 2% BSA. After several rinses in PBS, sections were incubated for 2 hours with a 1:200 dilution of secondary antibody donkey anti–goat-Cy3 (Jackson Immunoresearch, Newmarket, UK) in PBS-BSA. The preparations were rinsed again with PBS, counterstained using DAPI (Serva, Heidelberg, Germany), dried, and coverslipped. Control sections were treated without antibody, diluted and applied similarly to the specific antibody. Sections were studied by fluorescence microscopy using a photomicroscope equipped with epifluorescence (Axiophot; Zeiss, Jena, Germany).

Results

Imaging Osteolysis, Soft Tissue Tumor, and Vascularization in Bone Metastasis

With the aid of VCT, all relevant skeletal structures of both rat hind legs were imaged in high detail (Figure 1*A*). After injection of contrast agent, the arterial branching pattern of the legs such as the femoral, saphenous, and caudal femoral arteries as well as the plantar vessels was demonstrated (Figure 1*A*). After inoculation of MDA-MB-231 cells into the right superficial epigastric artery, bone metastasis was observed exclusively at the right hind leg. By VCT reconstruction, osteolyses became evident, such as that of the right fibula shown in Figure 1*A*. After injection of CT contrast agent, new vessel formation was visualized by VCT in the tumor-bearing leg only. Typically, these vessels branched off the femoral, saphenous, and caudal femoral arteries as shown in Figure 1*A*.

MRI revealed the surrounding soft tissue tumor, which usually exceeded the osteolytic lesion in size after intramedullar growth and penetration of cortical bone (Figure 1*B*). Furthermore, anatomic structures such as the pelvis, femur, tibia, and the surrounding muscles of the thighs were well depicted at sufficient quality on the same MR image (Figure 1*B*). In addition, the distribution of MR contrast agent was shown on MRI color maps with the amplitude *A* representing the relative increase in signal intensity as a surrogate marker for vascularization, which was expressed by the given color code as shown in Figure 1*B*. Low values for contrast agent uptake were found in the muscles of the lower extremities, the skin of the animal, and the bone marrow of the left hind leg (Figure 1*B*). In this soft tissue tumor of the right hind leg especially high values (color code, red) were displayed at the leading edge of the tumor but not in the tumor center or the surrounding muscle tissue. Histologic evaluation of this bone metastasis revealed highly vascularized

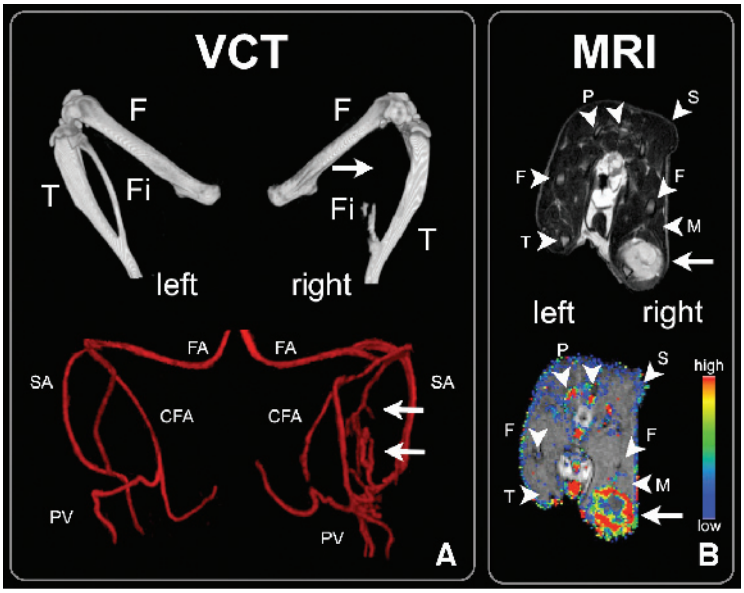

Figure 1. Corresponding images of VCT reconstructions (A) and MRI sequences (B) of a rat hind leg bone metastasis. (A) VCT images (upper row) of both hind legs illustrating the femur (F), tibia (T), and fibula (Fi). In the right hind leg, osteolytic destruction of the proximal fibula (arrow) is seen (upper row, right). Contrast-enhanced VCT image of the left hind leg (lower row, left) visualizes the major vessels such as the femoral artery (FA), saphenous artery (SA), caudal femoral artery (CFA), and plantar vessels. New vessel formation in the bone metastasis is indicated by arrows (lower row, right). (B) Axial T2–weighted MR image (upper row) and DCE MRI parameter map of the amplitude A (lower row) of a nude rat with arrowheads pointing to the femur (F), tibia (T), pelvis (P), skin (S), and muscles (M) and an arrow pointing to the tumor. The color code for the parameter map is ranging from blue (low values) to red (high values).

tumor tissue at the leading edge of the tumor and poorly vascularized or partly necrotic tissue in the center of the metastasis (data not shown).

Antiangiogenic Treatment with Bevacizumab

In this study, 17 control rats were compared with 15 rats treated with the VEGF antibody bevacizumab (Table 1). By VCT and MR imaging, the size of osteolytic lesions and soft tissue tumors as well as the respective amplitude *A* in bone metastases were followed from day 30 to day 70 after tumor cell inoculation (postinjection, p.i.) with an interval of 10 days. In animals of the treatment group, bevacizumab was injected weekly starting at day 35 until day 63 p.i. (Table 1).

According to the UICC criteria, treatment response of malignant lesions in bone can be defined as progressive disease (PD), no change (NC), and partial or complete remissions (PR and CR, respectively). When these criteria were applied to the bone metastases in this study, 12 animals (70.6%) of the control group and 1 animal (6.7%) of the treatment group showed progressive disease for their osteolytic lesions. In addition, 13 rats (76.5%) of the control group were diagnosed with a progressive soft tissue tumor compared with 3 animals (20.0%) of the treatment group (Table 1). No complete response was found after bevacizumab treatment. However, 8 (53.3%) and 6 (40.0%) rats experienced a partial remission or no change of osteolytic lesions in response to bevacizumab compared with 2 (11.8%) and 3 (17.6%) rats of the control group ($P < .001$, respectively). Similarly, 10 (66.7%) and 2 (13.3%) rats underwent a partial remission and no change, respectively, regarding their soft tissue tumor in response to the treatment compared with 1 (5.9%) and 3 (17.6%) animals of the control group, respectively ($P < .001$ for PR).

In control animals, the mean osteolytic lesion size increased constantly from day 30 to day 70 p.i. by 135% (Figure 2*A*). In comparison, this parameter increased only by 18% in the treatment group from days 30 to 50 and decreased afterward to 81% at day 70 p.i.

Table 1. Design of Experiment and Treatment Results.

	Animal No.	Treatment	Imaging	No. (%) of Animals with Osteolysis Showing				No. (%) of Animals with Soft Tissue Tumor Showing			
				PD	NC*	PR†	*T/C* (%)‡	PD	NC§	PR¶	*T/C* (%)‡
Control	17	0.9% NaCl#	VCT, MRI**	12 (70.6)	3 (17.6)	2 (11.8)	100	13 (76.5)	3 (17.6)	1 (5.9)	100
Bevacizumab	15	10 mg/kg bevacizumab††	VCT, MRI**	1 (6.7)	6 (40.0)	8 (53.3)	35	3 (20.0)	2 (13.3)	10 (66.7)	27

PD, progressive disease; NC, no change; PR, partial response; for definitions, see the Materials and Methods section.
*χ^2 test: PD versus NC, $P = .0035$.
†χ^2 test: PD versus PR, $P = .00043$ (PD vs NC + PR, $P = .00024$).
‡Ratio between treatment (*T*) and control (*C*) values in percent at day 70 after tumor cell inoculation; the respective means are given in Figure 2, *A* and *B*.
§χ^2 test: PD versus NC, $P = .33016$.
¶χ^2 test: PD versus PR, $P = .00023$ (PD vs NC + PR, $P = .00143$).
#Administered on the same day and at the same volume as bevacizumab.
**At days 30 to 70 after tumor cell inoculation every 10 days.
††IV application on days 35, 42, 49, 56, and 63 after tumor cell inoculation.

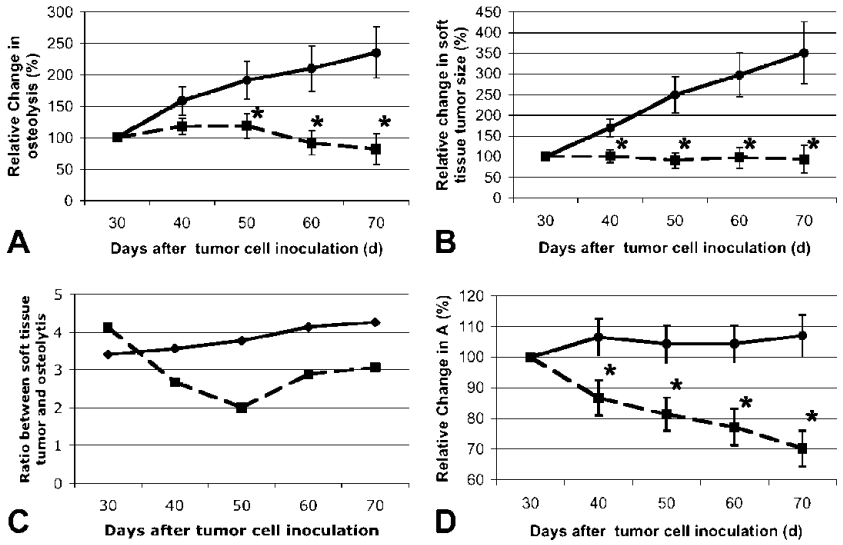

Figure 2. Comparison of control (solid line) and treated animals (dashed line). Mean values in percent of the relative change in osteolytic lesion size (A), soft tissue tumor size (B), and amplitude *A* values (D) versus time after tumor cell inoculation. (C) Ratio between size of the soft tissue tumor and osteolysis over time. Error bars indicate the standard error and asterisks denote a significant difference between groups ($P < .05$).

($P < .05$ vs control, Figure 2*A*). The mean size of control soft tissue tumors increased by 251% during the observation period, whereas that of the treatment group decreased by 7% of the initial values ($P < .05$ vs control, Figure 2*B*). The ratio between osteolytic lesion and soft tissue tumor sizes increased in controls from 3.4 to 4.3 (days 30 to 70) but decreased from 4.1 to 2.0 in treated animals (days 30 to 50) and increased thereafter to 3.1 (day 70 p.i., Figure 2*C*). The mean value for amplitude *A* in bone metastases of control rats remained almost constant (103% to 107%) during days 40 to 70 but decreased in the treatment group to 70% at day 70 p.i. of its initial value ($P < .05$ for days 40 to 70, Figure 2*D*).

The typical progression of sham-treated bone metastasis within the observation period (days 30 to 70) regarding osteolytic lesion development and corresponding increase in soft tissue tumor is recorded for an animal shown in Figure 3*A* (upper and middle rows). In these growing lesions, the amplitude *A* values increased in area but not

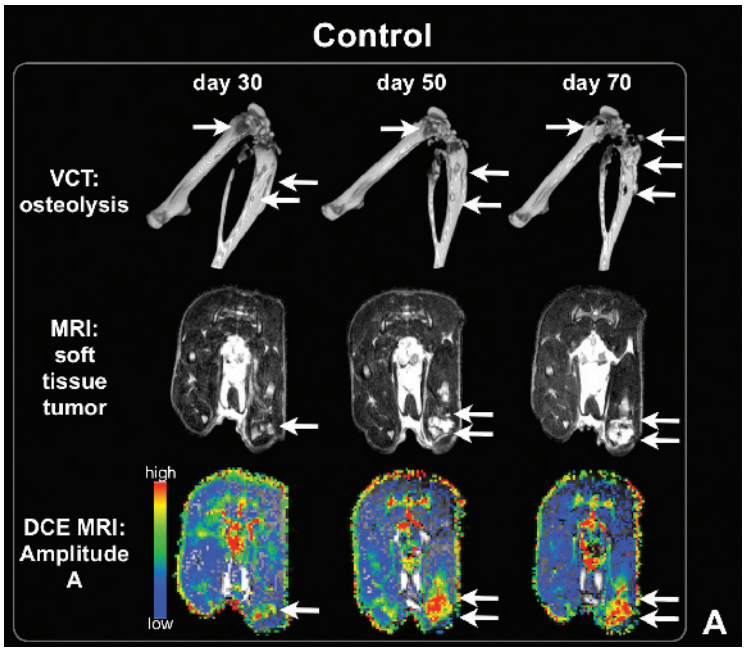

Figure 3. Monitoring by VCT and MRI of a control rat (control, A) and two treated rats (Responsive and Nonresponsive, B and C, respectively) at days 30, 50, and 70 after tumor cell inoculation. In the upper rows, osteolysis (arrows) of the right hind leg can be observed on VCT images of bone reconstructions. On T2-weighted axial MR images (middle rows) the change in soft tissue tumors (arrows) is shown over time. DCE MRI–derived parameter maps of the amplitude *A* are shown in the lower rows with values for *A* ranging from blue (low) to red (high); bone metastases are indicated by arrows.

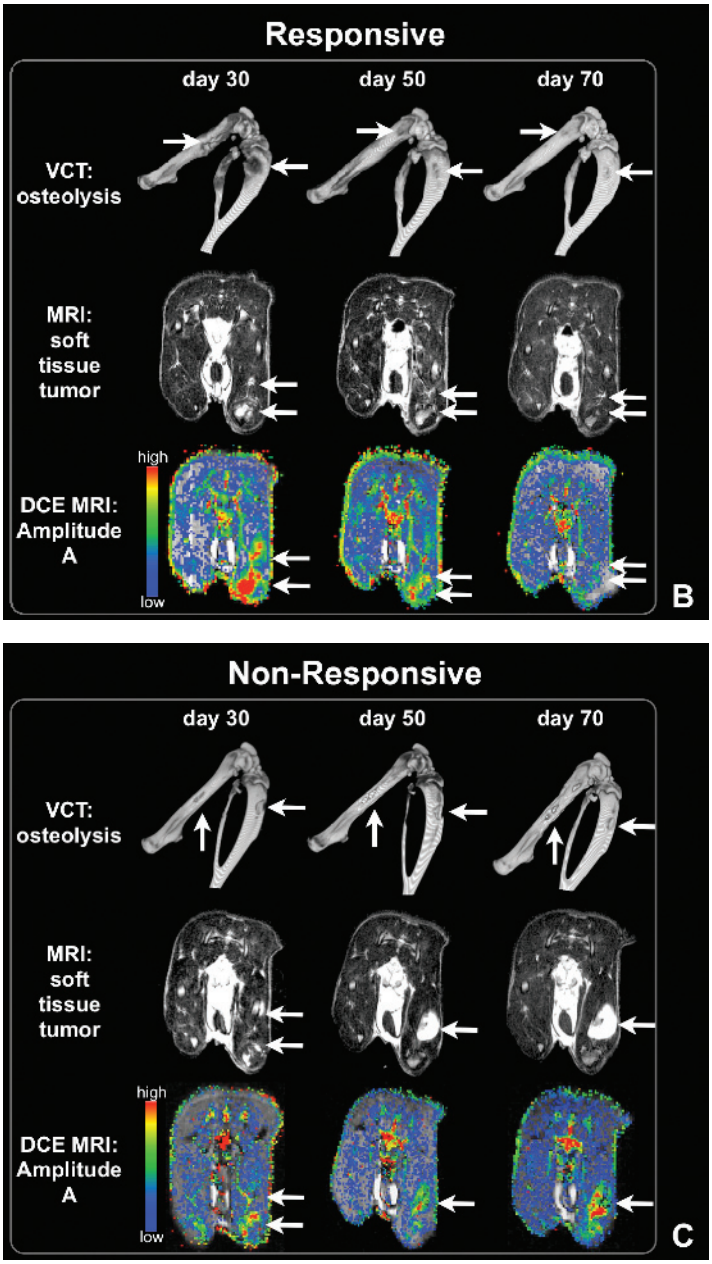

Figure 3. (*continued*)

in intensity as shown by the corresponding color maps (Figure 3*A*, lower row). In a treated animal, a partial remission of the osteolytic lesion and a corresponding decrease in the soft tissue tumor size was paralleled by a distinct reduction in amplitude *A* values at days 50 and 70 p.i. (upper, middle, and lower row, respectively; Figure 3*B*). To highlight both the most and the least intensive responses to treatment, one of three animals showing "no change" regarding its osteolysis is shown for comparison (upper row, Figure 3*C*). Remarkably, such a no-change status in the skeleton was in each case accompanied by a progression of the corresponding soft tissue tumor (middle row, Figure 3*C*). The respective amplitude *A* values were in line with the soft tissue tumor progression (lower row, Figure 3*C*).

Contrast-Enhanced VCT and Histologic Examination

At the end of the experiment, a final contrast-enhanced VCT was performed to image the arterial branching pattern of the tumor-bearing hind legs. As shown in Figure 4*A*, new vessel formation and change in vessel diameters as well as an altered branching pattern were most prominent in control animals but almost absent in treated rats. The mean number of newly formed vessels or vessels with an increased diameter was 4.5 in the control and 2.5 in the treatment group ($P < .05$, Figure 4*B*).

Histologic examination of the tumor-bearing leg in control rats revealed bone metastasis with MDA-MB-231 tumor cells in the bone marrow cavity stimulating osteolysis, infiltrating surrounding muscle tissue, and inducing new vessel formation (Figure 5, *A* and *C*). On immunohistochemical sections, MDA-MB-231 tumor cells were found within a tortuous network of tumor vessels (Figure 5*E*). After treatment with bevacizumab, new bone formation was found in the bone marrow of these animals (Figure 5, *B* and *D*). In comparison to sham-treated animals, only few viable tumor cells were left in the bone marrow without prominent vascularization (Figure 5*F*).

Discussion

Our aim was to evaluate treatment effects of the VEGF antibody bevacizumab in an experimental model of breast cancer bone metastasis. For this aim we imaged bone metastases by VCT and MRI to assess osteolysis, corresponding soft tissue tumor, and angiogenesis in these lesions of treated and control animals.

In most preclinical models of bone metastasis, either conventional X-rays or optical imaging of luciferase activity is used as a fast and cost-effective imaging method [14–16]. Optical imaging of bone metastasis is used for early diagnosis and semiquantitative monitoring of relative changes in soft tissue tumor size. A major drawback, however, is the lack of exact anatomic information and the fact that light emission from skeletal structures is influenced by the distance between the light-emitting cell and surface of the animal, as well as by the scattering caused by anatomic structures located in between. In contrast to optical imaging, conventional X-rays visualize mainly the skeletal effects elicited by bone-seeking tumor cells. Because only bone destruction of more than 50% can be detected with this technique it is considered a relatively insensitive measure of late skeletal changes [17]. Therefore, new technologies are needed to assess early changes of bone destruction, such as VCT, which has been developed as a fast and high-resolution imaging of anatomic structures in small animals [8]. For example, bone structures in mice were recorded with a resolution down to 200 μm [8,18]. Also, after contrast agent injection, tumor vessels of a diameter as low as 50 μm were visualized in subcutaneous tumors of mice [9]. Despite these qualities, a soft tissue tumor in the vicinity of skeletal lesions can hardly be assessed except after using contrast agent. Without contrast agent, MRI has been shown to detect the presence of a soft tissue tumor earlier than with X-rays [19]. Contrast-enhanced MRI is beginning to be used in preclinical studies to noninvasively image vascularization and treatment response by DCE MRI [20]. In this regard, high and low amplitude *A* values as surrogate markers for vascularization have been correlated to subcutaneous tumors with highly and poorly vascularized tumor areas, respectively [11].

In this study, by VCT all relevant skeletal structures of the hind legs and the extent of osteolysis could be followed during the observation period three dimensionally and in high resolution. MRI showed the anatomic location and extent of the soft tissue tumors, which clearly exceeded the lytic bone lesions. DCE MRI according to the pharmacokinetic model of Brix et al. [12] was used to image and quantify the distribution of contrast agent in bone metastasis. In these tumors, a strong uptake of contrast agent indicating high vascularization was observed. For these reasons, the combination of contrast-enhanced VCT and MRI is highly suitable for preclinical treatment studies of bone metastasis and in particular with antiangiogenic agents.

Treatment response to the anti-VEGF antibody bevacizumab was therefore followed noninvasively by VCT and MRI in this study. The amplitude *A* of DCE MRI in bone metastases remained largely unchanged in control animals but decreased significantly in the treatment group. This effect was paralleled by new bone formation and decreasing tumor vascularization as shown by VCT and histology. These results are in line with the findings of Kiessling et al., who observed a decrease in amplitude *A* as well as in microvessel density in subcutaneous heterotransplants of human skin squamous cell carcinomas after administration of a VEGF receptor antibody [21].

The assessment of disease response in patients with breast cancer bone metastasis is widely quantified according to the criteria of the UICC and the World Health Organization, which are based on plain radiography and skeletal scintigraphy [13,22]. The RECIST (response evaluation criteria for solid tumors) system, a more recent classification of tumor response, considers bone metastases as "non-measurable" [23]. In patients with bone metastases, DCE MRI was shown to be valuable in the differentiation of benign and malignant vertebral lesions [24]. In a small pilot study, signal-intensity curves measured by MRI after contrast agent injection differed before and after therapy with bisphosphonates and endocrine therapy in patients responding to the treatment [25]. Therefore DCE MRI and, according to the results of this study, the amplitude *A* can be considered a

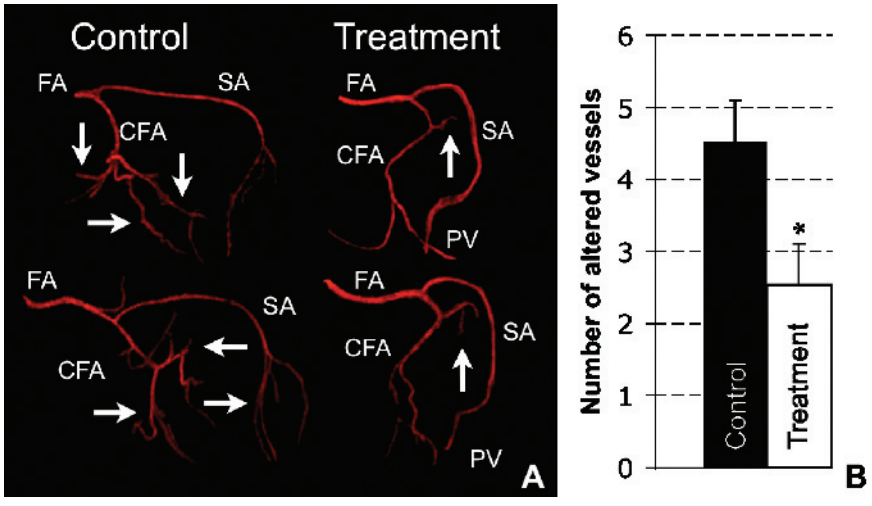

Figure 4. Alteration of the vessel branching pattern in tumor-bearing hind legs at day 70 after tumor cell inoculation. (A) Contrast-enhanced VCT images of tumor-bearing hind legs in two control (left column) and two treated (right column) rats. In tumor-bearing control animals, new vessel formation (arrows) branching off the femoral (FA), saphenous (SA), and caudal femoral arteries (CFA) is clearly present but almost absent in treated animals (arrows). (B) Mean number of altered vessels (newly formed vessels or vessels showing an increase in diameter) in control (black column) and treated animals (white column). Error bars indicate the standard error and the asterisk denotes a significant difference between the groups ($P < .05$).

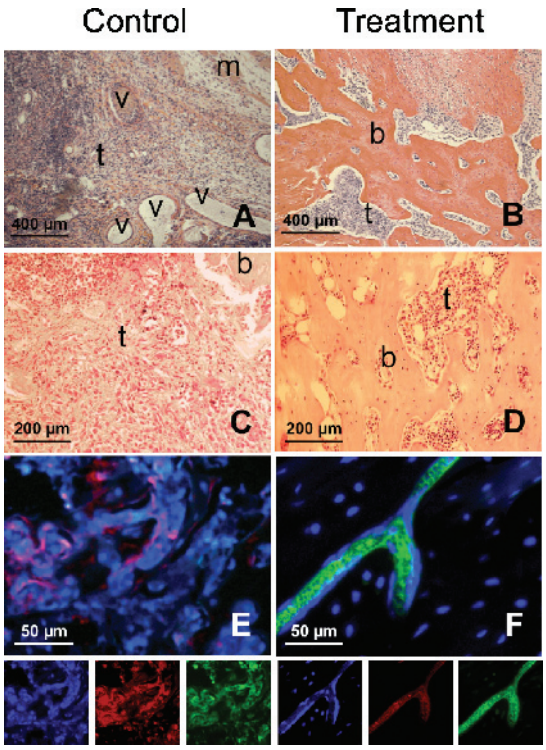

Figure 5. Histological comparison between bone metastasis in control (left column) and treated rats (right column). HE staining: highly vascularized (v, vessels) tumor (t) of MDA-MB-231 breast cancer cells infiltrating surrounding muscle tissue (m) (A). MDA-MB-231 tumor cells (t) within bone marrow cavity after lysis of cancellous bone (b, C). Osteogenesis in treated rats with remaining tumor cells (t) in between the newly formed bone (b, B and D). Immunohistology: merging of blue, red, and green color channels (green, MDA-MB-231 cells with GFP expression; blue, DAPI staining; red, CD-31 staining) showing MDA-MB-231 cells within a tortuous network of tumor vessels (E). Single remaining MDA-MB-231 cells within newly formed bone (black). The respective color channels (blue, red, and green) are shown below. Magnifications: 5-fold (A and B), 10-fold (C and D), and 40-fold (E and F).

valuable imaging parameter for noninvasive monitoring of treatment response in breast cancer bone metastasis.

Treatment with the VEGF antibody in nude rats caused partial remission according to the UICC classification in up to 67% of the animals, but had a different impact on osteolytic and soft tissue lesions. As bone lysis is a relatively slow process, it can be assumed that a treatment response is seen earlier in the soft tissue component of the metastatic process. This might be the reason for the earlier significant difference (day 40) in soft tissue metastasis between control and treated animals and the later treatment response (day 50) regarding osteolysis. This relation is reflected by the ratio over time between soft tissue and osteolytic lesion sizes, which indicates an early decrease in soft tissue lesion size after application of bevacizumab and a delayed treatment response of the osteolysis.

Our result that bone metastatic soft tissue tumors were reduced by 73% in comparison with control rats shows that this tumor entity reacts similarly as reported for subcutaneous or orthotopically growing transplanted tumors. In fact, various studies reported growth inhibition of human tumor xenografts of the breast, prostate, and brain ranging from 25% to 95% after inhibition of VEGF with bevacizumab [26]. Also, by a VEGF receptor-1–neutralizing antibody, the growth of human breast cancer MDA-MB-231 xenografts was significantly suppressed [27].

Inhibition of bone resorption caused by antiangiogenic treatment has been reported before when using the MDA-MB-231 model of breast cancer bone metastasis [28,29]. These groups hypothesized a direct inhibition of osteoclast activity and generation as causal factors of the antiosteoclastic effect resulting from their antiangiogenic molecules [28,29]. VEGF as one of the most import stimulators of angiogenesis is known to increase osteoclast-mediated bone resorption, to induce osteoclast chemotaxis, and to recruit osteoclasts to the site of bone remodeling [30,31]. In histologic sections of breast cancer bone metastasis of patients, the tumor cells strongly expressed VEGF and the surrounding osteoclasts were positive for VEGF receptors [32]. In the same study, peripheral blood mononuclear cells influenced by VEGF and receptor activator of nuclear factor kappa B ligand differentiated into osteoclast-like cells able to resorb bonelike substrate. Therefore, VEGF is a promising factor to stimulate angiogenesis as well as osteoclastic bone resorption. In line with this, the human breast cancer cell line MDA-MB-231 was reported to express high levels of VEGF-A and -B in bone and visceral metastasis [6]. Interestingly, the expression of VEGF-A and -B mRNA as well as bone resorption stimulators such as parathyroid hormone–related protein and macrophage colony–stimulating factor mRNA was significantly elevated in bone versus visceral metastasis [6]. There is evidence that transforming growth factor beta, another key player in the pathogenesis of bone metastasis, is responsible for tumor secretion of VEGF in breast cancer bone metastases [33,34].

Thus, several lines of evidence suggest that VEGF is associated with the expression of major bone-resorbing factors in breast cancer bone metastasis, such as transforming growth factor beta, parathyroid hormone–related protein, macrophage colony–stimulating factor, and nuclear factor kappa B ligand, and this association, in turn, highlights VEGF as an important osteolytic factor. Here we report that bevacizumab, an antibody against all human isoforms of VEGF, reduced osteolysis by 19% of the initial pretreatment size and by 65% compared to control animals. In 20% of the treated animals, soft tissue tumors progressed, whereas an unchanged osteolytic lesion size was observed. This observation fits well with the reported increased presence of VEGF mRNA in skeletal compared to visceral metastasis.

In the rat model used, new bone formation was observed after treatment with bevacizumab. This process requires VEGF for effective osteoblastic function [35]. It is plausible that two sources contributed to VEGF levels in tumor-bearing rats: In addition to the endogenous rat VEGF, human tumor cell–derived VEGF contributed to the effect observed. The inhibition of this latter VEGF activity by an antibody recognizing only human isoforms of VEGF has led to the observed antitumor effect. It might be speculated, however, that additional inhibition of the rat isoforms would have resulted in an even greater antitumor effect. In this regard, the model might have underestimated what could be possible in patients. Another aspect of the animal model is as follows: By repeating VCT scans, tumor-bearing rats were exposed to approximately 300 mGy (cumulative dose) [36]. Although far from causing lethal (5 to 7.6 Gy) or other side effects typical for radiation, such as anemia, this dose could have exerted a confounding therapeutic effect [37]. This is noteworthy in view of the observation that bevacizumab in combination with irradiation can elicit additive or even synergistic effects in treated patients [38].

Bevacizumab monotherapy in patients with metastatic breast cancer has modest antitumor activity [39]. However, in phase 3 trials, combination regiments of bevacizumab plus paclitaxel showed improved response rates and significantly prolonged progression-free survival as compared with paclitaxel alone [40,41]. So far, in patients with breast cancer bone metastasis, a monotherapy with bevacizumab has not been evaluated but appears to be a valuable treatment approach based on our results. As no complete remission was achieved with bevacizumab alone in this study, combination therapies with standard treatments for breast cancer bone metastasis such as chemotherapy, bisphosphonate therapy, and radiation therapy should be evaluated in patients with breast cancer bone metastasis.

In conclusion, we report a promising treatment approach in breast cancer bone metastasis with the VEGF antibody bevacizumab and describe imaging methods of monitoring these lesions with VCT and MRI. The combination of these methods in preclinical animal models for investigation of antiangiogenic treatments was shown to be highly suitable for monitoring all aspects of bone metastasis noninvasively. Administration of the VEGF antibody bevacizumab resulted in tumor response including inhibition of osteolysis of the corresponding soft tissue tumor and of angiogenesis in a preclinical model of breast cancer bone metastasis.

Acknowledgments

We thank K. Leotta for excellent technical assistance with the volumetric computed tomography. Furthermore, we thank Bracco ALTANA Pharma, Konstanz, Germany and Milan, Italy for providing Imeron 400 and for the technical support and valuable discussions.

References

[1] Coleman RE (1997). Skeletal complications of malignancy. *Cancer* **80**, 1588–1594.
[2] Mundy GR (2002). Metastasis to bone: causes, consequences and therapeutic opportunities. *Nat Rev Cancer* **2**, 584–593.
[3] Chavez-Macgregor M, Aviles-Salas A, Green D, Fuentes-Alburo A, Gomez-Ruiz C, and Aguayo A (2005). Angiogenesis in the bone marrow of patients with breast cancer. *Clin Cancer Res* **11**, 5396–5400.
[4] Ferrara N (2002). VEGF and the quest for tumour angiogenesis factors. *Nat Rev Cancer* **2**, 795–803.
[5] Voorzanger-Rousselot N, Juillet F, Mareau E, Zimmermann J, Kalebic T, and Garnero P (2006). Association of 12 serum biochemical markers of angiogenesis, tumour invasion and bone turnover with bone metastases from breast cancer: a cross-sectional and longitudinal evaluation. *Br J Cancer* **95**, 506–514.
[6] van der Pluijm G, Sijmons B, Vloedgraven H, Deckers M, Papapoulos S, and Lowik C (2001). Monitoring metastatic behavior of human tumor cells in mice with species-specific polymerase chain reaction: elevated expression of angiogenesis and bone resorption stimulators by breast cancer in bone metastases. *J Bone Miner Res* **16**, 1077–1091.
[7] Jackson A, O'Connor JP, Parker GJ, and Jayson GC (2007). Imaging tumor vascular heterogeneity and angiogenesis using dynamic contrast-enhanced magnetic resonance imaging. *Clin Cancer Res* **13**, 3449–3459.
[8] Greschus S, Kiessling F, Lichy MP, Moll J, Mueller MM, Savai R, Rose F, Ruppert C, Gunther A, Luecke M, et al. (2005). Potential applications of flat-panel volumetric CT in morphologic and functional small animal imaging. *Neoplasia* **7**, 730–740.
[9] Kiessling F, Greschus S, Lichy MP, Bock M, Fink C, Vosseler S, Moll J, Mueller MM, Fusenig NE, Traupe H, et al. (2004). Volumetric computed tomography (VCT): a new technology for noninvasive, high-resolution monitoring of tumor angiogenesis. *Nat Med* **10**, 1133–1138.
[10] Bäuerle T, Adwan H, Kiessling F, Hilbig H, Armbruster FP, and Berger MR (2005). Characterization of a rat model with site-specific bone metastasis induced by MDA-MB-231 breast cancer cells and its application to the effects of an antibody against bone sialoprotein. *Int J Cancer* **115**, 177–186.
[11] Kiessling F, Heilmann M, Vosseler S, Lichy M, Krix M, Fink C, Kiessling I, Steinbauer H, Schad L, Fusenig NE, et al. (2003). Dynamic T1-weighted monitoring of vascularization in human carcinoma heterotransplants by magnetic resonance imaging. *Int J Cancer* **104**, 113–120.
[12] Brix G, Semmler W, Port R, Schad LR, Layer G, and Lorenz WJ (1991). Pharmacokinetic parameters in CNS Gd-DTPA enhanced MR imaging. *J Comput Assist Tomogr* **15**, 621–628.
[13] Hayward JL, Carbone PP, Heusen JC, Kumaoka S, Segaloff A, and Rubens RD (1977). Assessment of response to therapy in advanced breast cancer. *Br J Cancer* **35**, 292–298.
[14] Blouin S, Basle MF, and Chappard D (2005). Rat models of bone metastases. *Clin Exp Metastasis* **22**, 605–614.
[15] Wetterwald A, van der Pluijm G, Que I, Sijmons B, Buijs J, Karperien M, Lowik CW, Gautschi E, Thalmann GN, and Cecchini MG (2002). Optical imaging of cancer metastasis to bone marrow: a mouse model of minimal residual disease. *Am J Pathol* **160**, 1143–1153.
[16] Henriquez NV, van Overveld PG, Que I, Buijs JT, Bachelier R, Kaijzel EL, Lowik CW, Clezardin P, and van der Pluijm G (2007). Advances in optical imaging and novel model systems for cancer metastasis research. *Clin Exp Metastasis* **24**, 699–705.
[17] Edelstyn GA, Gillespie PJ, and Grebbel FS (1967). The radiological demonstration of osseous metastases. Experimental observations. *Clin Radiol* **18**, 159–162.
[18] Missbach-Guentner J, Dullin C, Zientkowska M, Domeyer-Missbach M, Kimmina S, Obenauer S, Kauer F, Stuhmer W, Grabbe E, Vogel WF, et al. (2007). Flat-panel detector-based volume computed tomography: a novel 3D imaging technique to monitor osteolytic bone lesions in a mouse tumor metastasis model. *Neoplasia* **9**, 755–765.
[19] Gauvain KM, Garbow JR, Song SK, Hirbe AC, and Weilbaecher K (2005). MRI detection of early bone metastases in b16 mouse melanoma models. *Clin Exp Metastasis* **22**, 403–411.
[20] Kiessling F, Jugold M, Woenne EC, and Brix G (2007). Non-invasive assessment of vessel morphology and function in tumors by magnetic resonance imaging. *Eur Radiol* **17**, 2136–2148.
[21] Kiessling F, Farhan N, Lichy MP, Vosseler S, Heilmann M, Krix M, Bohlen P, Miller DW, Mueller MM, Semmler W, et al. (2004). Dynamic contrast-enhanced magnetic resonance imaging rapidly indicates vessel regression in human squamous cell carcinomas grown in nude mice caused by VEGF receptor 2 blockade with DC101. *Neoplasia* **6**, 213–223.
[22] World Health Organization (1979). *WHO Handbook for Reporting Results of Cancer Treatment.* World Health Organization Offset Publication, Geneva, Switzerland.
[23] Therasse P, Arbuck SG, Eisenhauer EA, Wanders J, Kaplan RS, Rubinstein L, Verweij J, Van Glabbeke M, van Oosterom AT, Christian MC, et al. (2000). New guidelines to evaluate the response to treatment in solid tumors. European Organization for Research and Treatment of Cancer, National Cancer Institute of the United States, National Cancer Institute of Canada. *J Natl Cancer Inst* **92**, 205–216.
[24] Chen WT, Shih TT, Chen RC, Lo HY, Chou CT, Lee JM, and Tu HY (2002). Blood perfusion of vertebral lesions evaluated with gadolinium-enhanced dynamic MRI: in comparison with compression fracture and metastasis. *J Magn Reson Imaging* **15**, 308–314.
[25] Montemurro F, Russo F, Martincich L, Cirillo S, Gatti M, Aglietta M, and Regge D (2004). Dynamic contrast enhanced magnetic resonance imaging in monitoring bone metastases in breast cancer patients receiving bisphosphonates and endocrine therapy. *Acta Radiol* **45**, 71–74.
[26] Gerber HP and Ferrara N (2005). Pharmacology and pharmacodynamics of bevacizumab as monotherapy or in combination with cytotoxic therapy in preclinical studies. *Cancer Res* **65**, 671–680.
[27] Wu Y, Hooper AT, Zhong Z, Witte L, Bohlen P, Rafii S, and Hicklin DJ (2006). The vascular endothelial growth factor receptor (VEGFR-1) supports growth and survival of human breast carcinoma. *Int J Cancer* **119**, 1519–1529.
[28] Peyruchaud O, Serre CM, NicAmhlaoibh R, Fournier P, and Clezardin P (2003). Angiostatin inhibits bone metastasis formation in nude mice through a direct anti-osteoclastic activity. *J Biol Chem* **278**, 45826–45832.
[29] Weber MH, Lee J, and Orr FW (2002). The effect of Neovastat (AE-941) on an experimental metastatic bone tumor model. *Int J Oncol* **20**, 299–303.
[30] Niida S, Kaku M, Amano H, Yoshida H, Kataoka H, Nishikawa S, Tanne K, Maeda N, Nishikawa S, and Kodama H (1999). Vascular endothelial growth factor can substitute for macrophage colony-stimulating factor in the support of osteoclastic bone resorption. *J Exp Med* **190**, 293–298.

[31] Engsig MT, Chen QJ, Vu TH, Pedersen AC, Therkidsen B, Lund LR, Henriksen K, Lenhard T, Foged NT, Werb Z, et al. (2000). Matrix metalloproteinase 9 and vascular endothelial growth factor are essential for osteoclast recruitment into developing long bones. *J Cell Biol* **151**, 879–889.

[32] Aldridge SE, Lennard TW, Williams JR, and Birch MA (2005). Vascular endothelial growth factor acts as an osteolytic factor in breast cancer metastases to bone. *Br J Cancer* **92**, 1531–1537.

[33] Donovan D, Harmey JH, Toomey D, Osborne DH, Redmond HP, and Bouchier-Hayes DJ (1997). TGF beta-1 regulation of VEGF production by breast cancer cells. *Ann Surg Oncol* **4**, 621–627.

[34] Guise TA and Chirgwin JM (2003). Transforming growth factor-beta in osteolytic breast cancer bone metastases. *Clin Orthop Relat Res* (415 Suppl.), S32–S38.

[35] Zelzer E and Olsen BR (2005). Multiple roles of vascular endothelial growth factor (VEGF) in skeletal development, growth, and repair. *Curr Top Dev Biol* **65**, 169–187.

[36] Bartling SH, Stiller W, Grasruck M, Schmidt B, Peschke P, Semmler W, and Kiessling F (2007). Retrospective motion gating in small animal CT of mice and rats. *Invest Radiol* **42**, 704–714.

[37] Bartling SH, Stiller W, Semmler W, and Kiessling F (2007). Small animal computed tomography imaging. *Curr Med Imaging Rev* **3**, 45–49.

[38] Senan S and Smit EF (2007). Design of clinical trials of radiation combined with antiangiogenic therapy. *Oncologist* **12**, 465–477.

[39] Cobleigh MA, Langmuir VK, Sledge GW, Miller KD, Haney L, Novotny WF, Reimann JD, and Vassel A (2003). A phase I/II dose-escalation trial of bevacizumab in previously treated metastatic breast cancer. *Semin Oncol* **30**, 117–124.

[40] Miller K, Wang M, Gralow J, Dickler M, Cobleigh M, Perez EA, Shenkier T, Cella D, and Davidson NE (2007). Paclitaxel plus bevacizumab versus paclitaxel alone for metastatic breast cancer. *N Engl J Med* **357**, 2666–2676.

[41] Miller KD, Chap LI, Holmes FA, Cobleigh MA, Marcom PK, Fehrenbacher L, Dickler M, Overmoyer BA, Reimann JD, Sing AP, et al. (2005). Randomized phase III trial of capecitabine compared with bevacizumab plus capecitabine in patients with previously treated metastatic breast cancer. *J Clin Oncol* **23**, 792–799.